Supplementary Material - Pattern-fluid interpretation of chemical turbulence

Christian Scholz[1,2,*], Gerd E. Schröder-Turk[1], Klaus Mecke[1]

[1] Theoretische Physik, Friedrich-Alexander Universität Erlangen-Nürnberg, Staudtstr. 7B, 91058 Erlangen, Germany
[2] 2. Physikalisches Institut, Universität Stuttgart, 70569 Stuttgart, Germany
∗ E-mail: c.scholz@physik.uni-stuttgart.de

1 Minkowski functionals

In general the Minkowski functionals correspond to curvature integrals defined on compact sets. In 2D these integrals correspond to the area V, the perimeter or boundary length S and the Euler characteristic χ, where χ is the number difference of connected components and connected holes of the set. By thresholding gray-scale images, Minkowski functionals can be used to characterize any type of scalar field, such as chemical concentration fields, density fields in statistical of even astrophysics. In order to characterize Turing Patterns, which correspond to continuous concentration fields, usually represented by gray-scale images, we introduce a threshold $0 \leq \rho \leq 1$ where $\rho = 0$ corresponds to the minimum and $\rho = 1$ to the maximum concentration. The patterns are then converted to binary images, where all concentrations below ρ correspond to the black and all concentrations above ρ correspond to the white phase, where the boundaries are the isocontours of the relative concentration ρ. For every image the Minkowski functionals are obtained by performing a vectorization using a marching square algorithm. From the resulting vectorized images V, S and χ can be obtained numerically minimizing discretization errors. Thus we obtain the Minkowski functionals as a function of ρ. V is rescaled by the total area A_0 of the image, S is rescaled by λ/A_0 and χ by λ^2/A_0, where λ is the wavelength of the pattern obtained from the Fourier transform, to account for possibly different resolutions of the patterns. The functional dependence of the Minkowski functionals on ρ is characteristic for patterns from a specific phase. As shown in Fig. 2(c) in the main manuscript, intuitively V decreases monotonously with ρ for both pattern types starting from an entire white phase ($V/A_0 = 1$) until patches of the black phase appear, which decrease the area fraction until the white area disappears ($V/A_0 = 0$). A striking difference between the patterns can be observed in S and χ, which is related to the topological symmetry of the patterns, or the lack thereof. For the hexagonal patterns S first increases with ρ up to a sharp maximum at $\rho \approx 0.2$. This maximum is related to the threshold where separated dots form without overlapping each other and therefore maximizing the boundary length. As ρ increases further these dots shrink and eventually disappear, so that S decreases monotonously. For the stripe patterns both phases are almost equally weighted, so that apart from the generic behavior $S(\rho = 0, 1) \approx 0$ a plateau is observed, where the pattern is composed of stripes that only differ in thickness, leaving the perimeter constant. This symmetry is also apparent in χ where for the stripe phase almost symmetric peaks with opposite signs about $\rho = 0.5$ are observed. These peaks correspond to a dominating interconnected white or black phase respectively, with $\chi = 0$ with equal numbers of black and white components in between. For the hexagonal pattern a sharp minimum is observed for low ρ, corresponding to a connected white cluster with small inclusions, while for increasing ρ a positive plateau can be seen. This corresponds to the white dots mentioned above that only decrease in size, leaving their number unchanged. For patterns from the LE model, the Minkowski functionals are almost identical for patterns from the same phase and do not depend strongly on the choice of a,b, as shown in Fig. S1, where we plot the Minkowski functionals for six patterns from the hexagonal and the stripe phase.

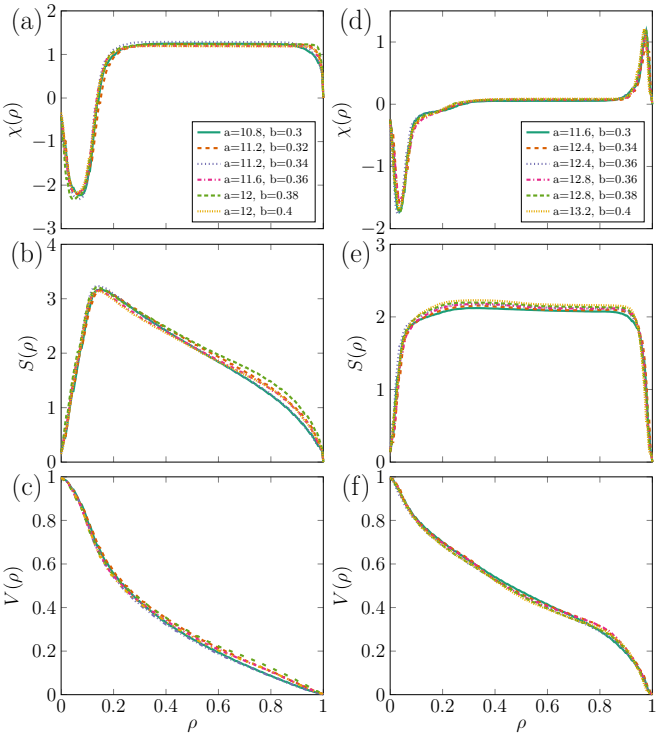

Fig. S1: **Minkowski functionals for hexagonal and stripe patterns from the LE model.** (a)-(c) Minkowski functionals for hexagonal patterns from the LE model for different values of a,b. $\sigma = 20$ remains constant for all patterns and similarly (d)-(f) Minkowski functionals for stripe patterns. The ρ dependence is characteristic for patterns from a certain phase. However only a small variation is found between the Minkowski functionals for different patterns from the same phase, when a and b are varied.

2 Pattern-Fluid for the Stripe Phase

Our observations shown for the hexagonal phase apply equally to the stripe phase observed in the CIMA reaction. Quantitative

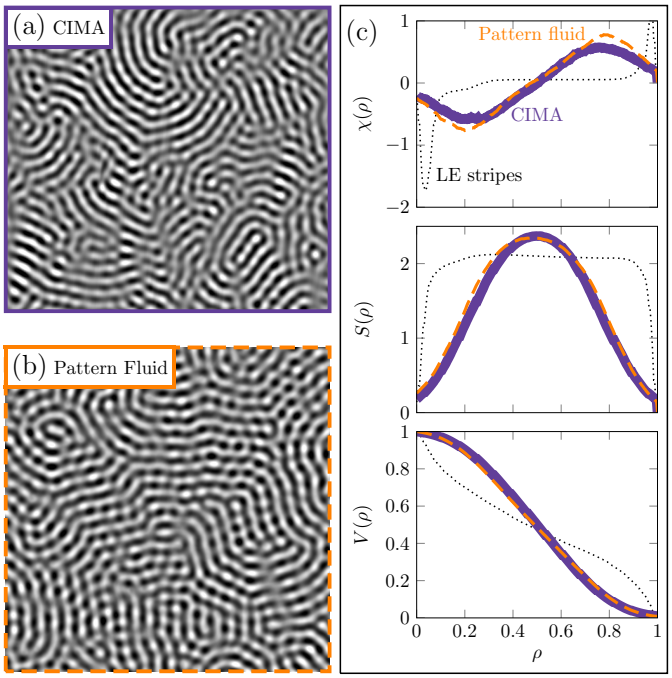

Fig. S3: **Substantial differences, quantified by morphometric Minkowski analysis, between the stationary stripe patterns in the CIMA reaction and the deterministic Lengyel-Epstein model are reconciled by the pattern-fluid model:** (a) Experimental stripe pattern from [1] at concentrations $[ClO_2^-]^A = 16\,\text{mM}$, $[H_2SO_4]^B = 6\,\text{mM}$, $[MA] = 9\,\text{mM}$. (b) Numerical pattern-fluid for $\phi = 0.225$, $N = 18$ (c) Minkowski functionals $V(\rho)$, $S(\rho)$ and $\chi(\rho)$ of stationary numerical stripe LE pattern (dots), experimental CIMA pattern (solid) from (a) and pattern-fluid (dashed) from (b).

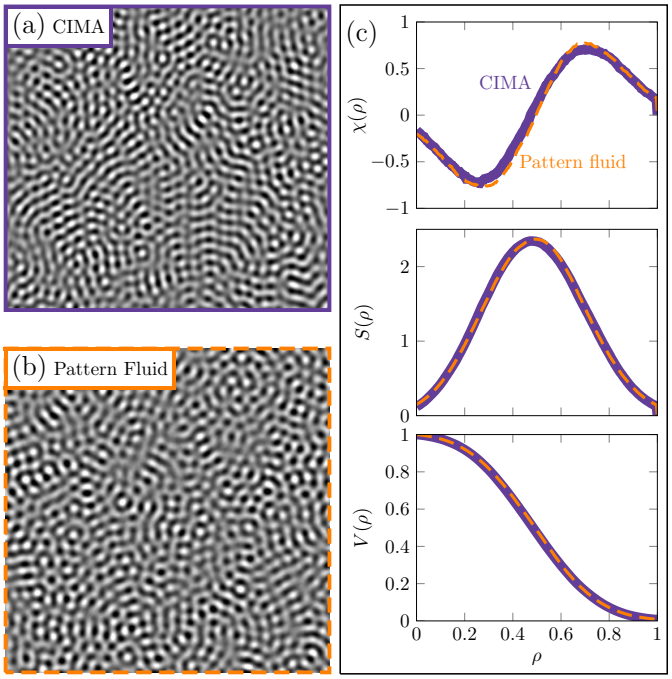

Fig. S4: **Morphometric Minkowski analysis of experimental concentration profiles of the turbulent CIMA phase with the high-temperature phase of the pattern-fluid model:** (a) Experimental turbulent pattern from [1, 2] with malonic acid concentration $[ClO_2^-]^A = 18\,\text{mM}$, $[H_2SO_4]^B = 10\,\text{mM}$, $[MA] = 9\,\text{mM}$. See [1] for initial chemical concentrations. (b) Numerical pattern-fluid according to Eq. (3) with $\phi = 0.05, N = 14$. (c) area V/A_0, perimeter $S\lambda/A_0$ and Euler Characteristic $\chi\lambda^2/A_0$ as a function of ρ for the experimental turbulence (solid) and numerical pattern-fluid patterns (dashed) from (a),(b).

differences between the deterministic LE model stripe patterns and those from the CIMA reaction can be understood by the application of the pattern-fluid model. An overlap of stripe patterns is found to reproduce the turbulent patterns found in the experiment close to the transition to the stripe phase. Similar to the analysis of the hexagonal phase in order to find suitable parameter sets for ϕ and N we compare the Minkowski functionals for $\bar{u}$ and selected experimental patterns from the turbulent and stationary phases with a ground state u_0 from the stripe phase ($a = 12$, $b = 0.275$). The turbulent CIMA pattern has been selected from a part of the phase space, close to the transition from stripes to turbulence. Similar to the hexagonal phase we find a good agreement for the turbulent phase for large N and small ϕ. Again for the stationary stripe patterns the morphological agreement is improved significantly for non-zero values of N and $\phi < 1$ (See Figs. S2 and S3). Additionally the turbulent CIMA patterns close to the transition to stationary stripes are well reproduced by a pattern-fluid based on a fundamental stripe pattern with the appropriate parameters N, ϕ (See Figs. S2 and S4).

Supplementary References

[1] Ouyang, Q. and Swinney, H. L., Chaos **1** (1991) 411 .
[2] Mecke, K. R., Phys. Rev. E **53** (1996) 4794 .

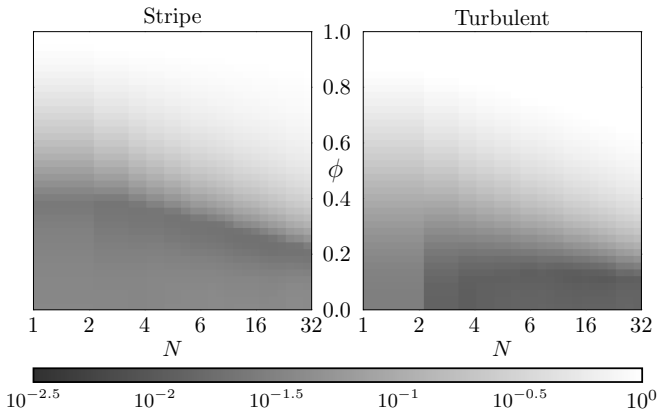

Fig. S2: **Determination of optimal parameter values for ground state occupancy ϕ and N in pattern-fluid model by minimizing the mean-squared difference Δ between Minkowski functionals of simulated and experimental images:** $\Delta = \max(\Delta V, \Delta S, \Delta\chi)$ for numerical pattern-fluid (averaged over 10 realizations) as a function of ϕ, N and for a stripe ground state u_0 ($\sigma = 20, a = 12, b = 0.3$) compared to CIMA patterns from [1] for (left) stripe phase $[ClO_2^-]^A = 16\,\text{mM}$, $[H_2SO_4]^B = 6\,\text{mM}$, $[MA] = 9\,\text{mM}$ and (right) turbulence $[ClO_2^-]^A = 18\,\text{mM}$, $[H_2SO_4]^B = 10\,\text{mM}$, $[MA] = 9\,\text{mM}$.